

ONLINE FDR CONTROLLING PROCEDURES FOR STATISTICAL SIS MODEL AND ITS APPLICATION TO COVID19 DATA

BY SEOHWA HWANG¹, JUNYONG PARK^{1,a}

¹Department of Statistics, Seoul National University, ^ajumyongpark@snu.ac.kr

We propose an online false discovery rate (FDR) controlling method based on conditional local FDR (LIS), designed for infectious disease datasets that are discrete and exhibit complex dependencies. Unlike existing online FDR methods, which often assume independence or suffer from low statistical power in dependent settings, our approach effectively controls FDR while maintaining high detection power in realistic epidemic scenarios. For disease modeling, we establish a Dynamic Bayesian Network (DBN) structure within the Susceptible-Infected-Susceptible (SIS) model, a widely used epidemiological framework for infectious diseases. Our method requires no additional tuning parameters apart from the width of the sliding window, making it practical for real-time disease monitoring. From a statistical perspective, we prove that our method ensures valid FDR control under stationary and ergodic dependencies, extending online hypothesis testing to a broader range of dependent and discrete datasets. Additionally, our method achieves higher statistical power than existing approaches by leveraging LIS, which has been shown to be more powerful than traditional p -value-based methods. We validate our method through extensive simulations and real-world applications, including the analysis of infectious disease incidence data. Our results demonstrate that the proposed approach outperforms existing methods by achieving higher detection power while maintaining rigorous FDR control.

1. Introduction. Monitoring infectious disease spread in real time is a central task in public health surveillance. During the COVID-19 pandemic, many countries released daily confirmed case counts, requiring policymakers to determine when to escalate or relax interventions such as social distancing. However, short-term increases in reported cases do not always indicate a true surge in transmission: transient fluctuations caused by reporting delays or day-of-week effects can obscure the underlying trend.

For instance, daily increases in incidence may occur even amid an overall decline, while true upward trends may be hidden by noise or administrative lags. Relying on ad-hoc thresholds or short-term fluctuations to guide policy decisions can lead to premature or delayed responses, emphasizing the need for statistically rigorous tools that distinguish sustained increases from random variation. This paper introduces a robust statistical framework that integrates online FDR controlling procedures with a probabilistic formulation of the Susceptible-Infected-Susceptible (SIS) epidemiological model, structured within a Dynamic Bayesian Network (DBN). This synthesis allows for the sequential analysis of incoming data to test, in real-time, whether the number of observed cases is increasing, all while rigorously controlling for the proportion of false discoveries among all rejected hypotheses. The effectiveness and statistical properties of our proposed methods, in terms of both FDR control and power to detect true increases, are first validated through extensive simulation studies.

To demonstrate the practical utility and broad applicability of our framework, we conduct a comprehensive real-world data analysis using datasets from sources like Our World

Keywords and phrases: Online FDR, Susceptible-Infected-Susceptible model, Dynamic Bayesian Network, COVID-19.

in Data. Our analysis includes a deliberately diverse set of infectious diseases: COVID-19, influenza, chickenpox, *Mycoplasma pneumoniae*, Dengue Fever, Hand, Foot, and Mouth Disease (HFMD), and Hepatitis E. This selection allows for a robust evaluation of our method’s performance across varied epidemiological contexts, including different transmission mechanisms and data reporting structures.

The application of our model to this diverse set of pathogens serves two key purposes. First, it tests the model’s performance across various transmission dynamics. For diseases characterized primarily by direct person-to-person contact where reinfection is possible (COVID-19, influenza, HFMD, chickenpox), the SIS model is a fundamentally well-suited framework. For diseases with more complex transmission pathways, such as the vector-borne Dengue Fever or the waterborne Hepatitis E, our application of the SIS model tests its utility as a robust, first-order surveillance tool. In these cases, the model’s transmission parameter acts as an effective aggregate measure that captures the net result of the more complex underlying epidemiological processes, even without explicitly modeling vectors or environmental reservoirs. Second, this disease selection inherently includes data with different temporal granularities, from daily reporting (e.g., COVID-19) to weekly reporting (e.g., influenza, Dengue Fever). This variation allows us to demonstrate the flexibility of our online procedure, which is designed to sequentially process observations as they arrive, regardless of the specific time interval between them. This highlights its practical value for real-world public health data streams, which are often inconsistent in their reporting frequency.

The remainder of this paper is organized as follows. Section 2 reviews the limitations of classical SIS models and existing online FDR-controlling procedures. Section 3 introduces a stochastic reformulation of the SIS model and describes how we modify its structure to enable statistical inference and hypothesis testing. Section 4 presents our proposed online testing procedure, which leverages temporal dependence through a latent-state framework to enhance detection power, and establishes its theoretical properties. Section 5 reports simulation results under various scenarios, including cases with seasonal effects and model misspecification. Section 6 provides a real data analysis on infectious diseases with diverse infection durations and transmission routes, demonstrating the practical utility of our method. Concluding remarks and directions for future work are provided in Section 7.

2. Literature Review.

2.1. Limitations of Classical SIS for Real-Time Monitoring. The Susceptible–Infectious–Susceptible (SIS) model is a classical framework used to describe the spread of infectious diseases (Kermack and McKendrick, 1927a). It partitions a fixed population of size N into susceptible individuals S_t and infected individuals \mathbb{I}_t at each time t . Infections occur through contact with the infected, and recovered individuals return to the susceptible pool.

Under a discrete-time formulation, the dynamics evolve via:

$$(2.1) \quad S_{t+1} = S_t - S_t \cdot \frac{\tilde{\gamma}\mathbb{I}_t}{N} + \frac{1}{d}\mathbb{I}_t,$$

$$(2.2) \quad \mathbb{I}_{t+1} = S_t \cdot \frac{\tilde{\gamma}\mathbb{I}_t}{N} + \left(1 - \frac{1}{d}\right)\mathbb{I}_t,$$

where $\tilde{\gamma}$ is the per-contact transmission rate, and $1/d$ is the recovery rate corresponding to an average infectious duration of d days.

While useful for long-term forecasting, this deterministic model assumes a constant transmission rate over time and lacks flexibility for real-time inference. In practical surveillance settings, policymakers often ask a simpler question: Is the epidemic currently accelerating? That is, does the effective reproduction number $\gamma_t := d\tilde{\gamma}_t$ exceed 1 at time t ?

A natural formulation is the sequence of hypotheses:

$$H_{0t} : \gamma_t \leq 1 \quad \text{vs.} \quad H_{1t} : \gamma_t > 1.$$

However, testing this hypothesis directly is problematic. Estimating γ_t using the plug-in ratio $\hat{\gamma}_t = J_t/I_t$ (where J_t is the number of new infections and I_t an estimate of current infectious individuals per day) reduces the hypothesis test to a trivial threshold comparison between J_t and I_t : if $J_t \gg I_t$, H_{0t} is rejected, which ignores temporal structure or uncertainty.

2.2. *Dynamic Bayesian Networks (DBNs)*. A Dynamic Bayesian Network (DBN) is a probabilistic graphical model that extends the formalism of Bayesian Networks (BNs) to represent and reason about temporal processes. While a standard BN models the probabilistic dependencies among a set of variables at a single point in time, a DBN provides a compact representation of the joint probability distribution over sequences of variables evolving through time (Murphy, 2002).

Formally, a DBN models the distribution over a collection of time-indexed random variables $Z_t = \{Z_t^1, \dots, Z_t^n\}$. The model is defined by a pair of a prior network and a transition network.

1. **A prior network**, specifies the joint probability distribution over the state variables for the initial time steps required by the model’s dependency structure.
2. **A transition network**, defines the conditional probability distribution of the state variables at time t given the state over the d preceding time steps, denoted as $P(Z_t | Z_{t-d}, \dots, Z_{t-1})$.

In this work, we generalize the conventional first-order dependency and employ a d th-order Markov assumption, where the state of the system at time t is conditionally independent of the distant past given the states of the previous d time steps (Murphy, 2002). That is, for $t \geq d$:

$$(2.3) \quad P(Z_t | Z_0, \dots, Z_{t-1}) = P(Z_t | Z_{t-d}, \dots, Z_{t-1})$$

The transition network’s parameters and structure are assumed to be time-invariant (stationary), meaning the rules governing the system’s evolution do not change over time. By unrolling this network over T time steps, the DBN defines a full joint probability distribution over the trajectory $Z_{0:T} \equiv \{Z_0, Z_1, \dots, Z_T\}$ (Koller and Friedman, 2009).

The selection of the DBN framework for our method is motivated by several key advantages that directly facilitate our proposed methodology. First, the graphical structure of a DBN provides an intuitive and explicit representation of the model’s underlying assumptions. This visual clarity enhances interpretability, making the causal relationships between variables—such as the infectious pool (\mathbb{I}_t), the latent trend (θ_t), and new infections (J_t)—transparent. Second, DBNs offer a natural framework for integrating latent variables. This is crucial for our method, where the central hypothesis revolves around inferring an unobservable epidemic trend, θ_t . The DBN formalizes this trend as a hidden state within a generative process, allowing us to reason about the underlying dynamics driving the observable case counts.

Finally, and most critically, the DBN structure provides a principled and computationally tractable foundation for probabilistic inference. The explicitly defined dependencies allow for the application of efficient, exact algorithms for tasks such as filtering and smoothing. For our method, this is a paramount benefit, as the framework enables the use of the forward-backward algorithm to compute the posterior probability of the latent state, $P(\theta_t | J_1, \dots, J_T)$. This probability is essential as it forms the basis of the Local Index of Significance (LIS), the core test statistic for our online FDR controlling procedure (Efron,

2005; Sun and Cai, 2007). Therefore, the DBN acts as the crucial computational engine that makes our statistical tests feasible.

Due to their capacity to model temporal dependencies and incorporate latent (unobserved) variables, DBNs are exceptionally well-suited for modeling complex dynamic systems, including those found in epidemiology. In this work, the DBN framework is leveraged to represent the stochastic Susceptible-Infected-Susceptible (SIS) dynamics and to perform inference on a latent state variable representing the underlying epidemic trend.

2.3. Online Testing. A widely studied framework for online false discovery rate (FDR) control is the alpha-investing algorithm introduced by Foster and Stine (2008). This approach allocates a pre-specified "alpha-wealth" budget across sequential hypothesis tests. When a test results in a rejection, the procedure earns back some alpha wealth, enabling it to continue testing. This adaptive strategy allows for real-time updates to the significance level while maintaining FDR control.

Subsequent works have extended the alpha-investing framework. In particular, methods such as LORD++ (Ramdas et al., 2017a), SAFFRON (Ramdas et al., 2018), and ADDIS (Tian and Ramdas, 2019) reward successful rejections by dynamically increasing the alpha budget. These approaches offer greater flexibility and statistical power compared to static procedures.

Despite their innovation, alpha-investing algorithms suffer from well-documented issues such as alpha-death (where no new rejections occur due to a depleted alpha budget) and piggybacking (where large alpha rewards lead to overly aggressive rejections) (Ramdas et al., 2017b). To mitigate these challenges, Gang, Sun and Wang (2023) proposed the Structure-Adaptive Sequential Testing (SAST) framework, which builds on the conditional local index of significance (LIS) and adapts testing thresholds based on local structure in the data. SAST achieves FDR control under independence and offers near-optimal power in various structured testing scenarios.

Nonetheless, SAST assumes independence among test statistics, an assumption often violated in real-world applications such as infectious disease surveillance, where strong temporal dependence is intrinsic to the data. In such settings, modeling this dependence is critical for reliable detection.

3. Modeling Framework Motivated by Classical Infectious Disease Model.

3.1. Stochastic Modeling of Case Counts. We formulate a stochastic version of the SIS model. Define:

- J_t : the number of new infections at time t ;
- I_t : the rolling average of recent infections,

$$I_t = \frac{1}{\min(d, t)} \sum_{i=\max(t-d+1, 1)}^t J_i,$$

as a proxy for the infectious pool;

- $S_t = N - I_t$: the number of susceptibles, under the assumption $I_t \ll N$.

Given these quantities, we model J_t as:

$$J_t \mid (I_t, \gamma_t) \sim \text{Binomial} \left(S_t, \frac{\gamma_t I_t}{N} \right),$$

and under the standard Poisson approximation (valid when $S_t \approx N$), we write:

$$J_t \mid (I_t, \gamma_t) \approx \text{Poisson}(\gamma_t I_t).$$

This formulation captures daily randomness in case counts while linking them mechanistically to latent transmission dynamics.

The infectious pool is updated via a renewal equation:

$$I_{t+1} = I_t + J_t - J_{t-d+1},$$

which reflects that individuals remain infectious for d days before recovering.

3.2. Latent Trend Modeling via Hidden States. To overcome the instability of estimating γ_t for every t , we introduce a discrete latent state process $\theta_t \in \{1, 2, 3\}$ that governs the transmission regime. Specifically:

- $\theta_t = 1$: decreasing ($\gamma_t < 1$),
- $\theta_t = 2$: stationary ($\gamma_t = 1$),
- $\theta_t = 3$: increasing ($\gamma_t > 1$).

Conditionally on $\theta_t = j$, the transmission rate is modeled as:

$$\gamma_t \mid (\theta_t = j) \equiv \gamma_j$$

The hidden state sequence $\{\theta_t\}$ evolves according to a first-order Markov chain with transition matrix $A = [a_{ij}]_{1 \leq i, j \leq 3}$ and initial distribution $\pi = \{\pi_1, \pi_2, \pi_3\}$ as described in Figure 1. This latent-state framework defines a dynamic Bayesian network (DBN) over $\{\theta_t, \gamma_t, J_t\}$

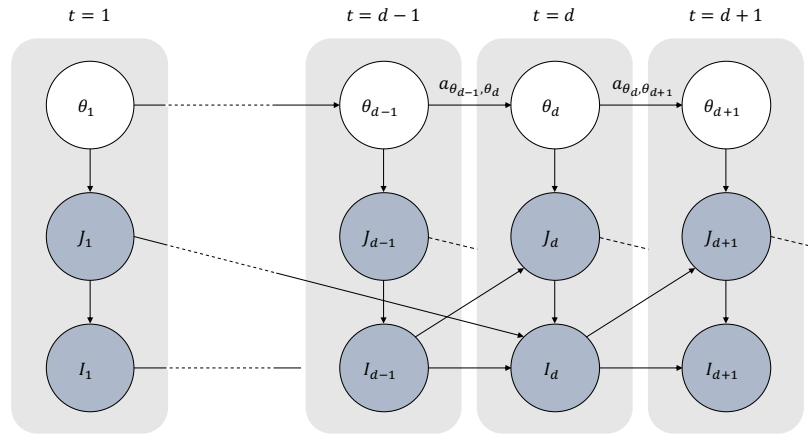


FIG 1. Dynamic Bayesian network (DBN) for the proposed model with latent state sequence $\{\theta_t\}_{t \geq 1}$. The initial distribution is $P(\theta_1 = i) = \pi_i$ for $i \in \{1, 2, 3\}$, and the transition law is $P(\theta_{t+1} = i \mid \theta_t = j) = a_{ij}$ for $i, j \in \{1, 2, 3\}$.

and allows for posterior inference via EM and forward-backward algorithms. It captures time-varying epidemic trends while avoiding day-to-day overfitting.

3.3. Statistical Hypothesis Testing Based on Posterior Inference. Instead of testing directly on γ_t , we test the latent trend state:

$$H_{0t} : \theta_t \in \{1, 2\} \quad \text{vs.} \quad H_{1t} : \theta_t = 3.$$

This reframing allows us to use Bayesian posterior probabilities to drive decisions. Let \mathcal{D}_t denote observed data in a window prior to time t , and define the local index of significance (LIS):

$$L_t := \mathbb{P}(\theta_t \in \{1, 2\} \mid \mathcal{D}_t),$$

as a probabilistic measure of evidence against the alternative. A small value of L_t suggests strong evidence that $\theta_t = 3$, indicating a supercritical trend.

This probabilistic formulation provides a natural test statistic for real-time monitoring and enables control of the false discovery rate (FDR) over time using recent advances in online multiple testing, as we detail in Section 4.

4. Proposed Method. Building on the latent-state SIS model introduced in Section 2.1, we now describe how to implement this framework for real-time epidemic monitoring. Our goal is to sequentially test for increases in transmission while controlling the false discovery rate (FDR) across time. This section details the statistical model, parameter estimation via the EM algorithm, and an online testing procedure based on Structure-Adaptive Sequential Testing (SAST⁺).

4.1. *Preprocessing via STL Decomposition (Optional).* To remove weekly seasonality in the raw incidence data J_t , we apply Seasonal-Trend Decomposition using LOESS (STL) (Cleveland et al., 1990). We decompose the log-intensity $\log \gamma_t$ into:

$$\log \gamma_t = T_t + S_t,$$

where T_t captures the long-term trend and S_t the seasonal component. To focus estimation on the trend, we adjust I_t by rescaling:

$$\tilde{I}_t := I_t \cdot \exp(S_t),$$

and treat $\gamma_t \tilde{I}_t$ as the effective Poisson mean. This preprocessing isolates trend-driven deviations.

4.2. *Parameter Estimation via the EM Algorithm.* We estimate the model parameters

$$(4.1) \quad \boldsymbol{\nu} = \{(\gamma_j)_{1 \leq j \leq 3}, (A_{ij})_{1 \leq i, j \leq 3}, (\pi_j)_{1 \leq j \leq 3}\}$$

via the Expectation-Maximization (EM) algorithm. Given the observed data $\{J_t, I_t\}_{t=1}^T$ and the latent epidemic state $\{\theta_t\}_{t=0}^T$, the complete-data likelihood under parameter $\boldsymbol{\nu}$ is given by:

$$(4.2) \quad P_{\boldsymbol{\nu}}(J_{1:T}, \theta_{1:T}) = \pi_{\theta_1} \cdot \prod_{t=2}^T A_{\theta_{t-1}, \theta_t} \cdot \prod_{t=1}^T \text{Poisson}(J_t; \gamma_{\theta_t} I_t).$$

The EM algorithm alternates between the following steps until convergence:

E-step. Compute the expected complete-data log-likelihood under the current parameter $\boldsymbol{\nu}^{(m)}$:

$$(4.3) \quad \begin{aligned} \mathcal{Q}(\boldsymbol{\nu}^{(m+1)} | \boldsymbol{\nu}^{(m)}) &= \mathbb{E}_{\boldsymbol{\nu}^{(m)}} [\log \mathbb{P}_{\boldsymbol{\nu}^{(m+1)}}(J_{1:T}, \theta_{1:T}) | J_{1:T}] \\ &= \sum_{j=1}^3 \mathbb{P}(\theta_1 = j | J_{1:T}) \cdot \log \pi_j^{(m+1)} \\ &\quad + \sum_{i,j=1}^3 \sum_{t=1}^T \mathbb{P}(\theta_{t-1} = i, \theta_t = j | J_{1:T}) \cdot \log A_{ij}^{(m+1)} \\ &\quad + \sum_{j=1}^3 \sum_{t=1}^T \mathbb{P}(\theta_t = j | J_{1:T}) \cdot \left\{ -\gamma_j^{(m+1)} I_t + J_t \log(\gamma_j^{(m+1)} I_t) - \log(J_t!) \right\}. \end{aligned}$$

To compute the marginal and joint posteriors of θ_t , we apply the forward-backward algorithm. Let $\alpha_i(t)$ and $\beta_i(t)$ be the forward and backward probabilities defined as:

$$(4.4) \quad \alpha_i(t) = \mathbb{P}(J_{1:t}, \theta_t = i) = \left(\sum_{j=1}^3 \alpha_j(t-1) A_{ji} \right) \cdot \text{Poisson}(J_t; \gamma_i I_t),$$

$$(4.5) \quad \beta_i(t) = \mathbb{P}(J_{t+1:T} | \theta_t = i) = \sum_{j=1}^3 A_{ij} \cdot \text{Poisson}(J_{t+1}; \gamma_j I_{t+1}) \cdot \beta_j(t+1),$$

with initialization

$$\alpha_i(1) = \pi_i \cdot \text{Poisson}(J_1; \gamma_i I_1), \quad \beta_i(T) = 1.$$

The marginal posterior is then computed by

$$(4.6) \quad \mathbb{P}(\theta_t = i | J_{1:T}) = \frac{\alpha_i(t) \cdot \beta_i(t)}{\sum_{j=1}^3 \alpha_j(t) \cdot \beta_j(t)}.$$

The joint posterior is given by:

$$(4.7) \quad \mathbb{P}(\theta_t = i, \theta_{t+1} = j | J_{1:T}) = \frac{\alpha_i(t) \cdot A_{ij} \cdot \text{Poisson}(J_{t+1}; \gamma_j I_{t+1}) \cdot \beta_j(t+1)}{\sum_{k,l} \alpha_k(t) \cdot A_{kl} \cdot \text{Poisson}(J_{t+1}; \gamma_l I_{t+1}) \cdot \beta_l(t+1)}.$$

M-step. Using the posterior estimates from the E-step, we update the parameters in closed form:

$$(4.8) \quad \pi_j^{(m+1)} = \mathbb{P}_{\nu^{(m)}}(\theta_1 = j | J_{1:T}),$$

$$(4.9) \quad A_{ij}^{(m+1)} = \frac{\sum_{t=1}^T \mathbb{P}_{\nu^{(m)}}(\theta_{t-1} = i, \theta_t = j | J_{1:T})}{\sum_{t=1}^T \mathbb{P}_{\nu^{(m)}}(\theta_{t-1} = i | J_{1:T})},$$

$$(4.10) \quad \gamma_j^{(m+1)} = \frac{\sum_{t=1}^T \mathbb{P}_{\nu^{(m)}}(\theta_t = j | J_{1:T}) \cdot J_t}{\sum_{t=1}^T \mathbb{P}_{\nu^{(m)}}(\theta_t = j | J_{1:T}) \cdot I_t}.$$

These updates are derived by maximizing each component of the Q-function (4.3), subject to the normalization constraints on π and A . Full derivations are provided in the supplementary material. The EM procedure iterates between computing (4.6)–(4.7) and applying the closed-form updates (4.8)–(4.10) until convergence. The complete algorithm is summarized in Algorithm 1, and additional details of the EM procedure are given in Appendix ??.

Algorithm 1: EM Algorithm for statSIS model

Input : Observed data $\{J_t, I_t\}_{t=1}^T$, initial parameters $\boldsymbol{\nu}^{(0)} = (\pi^{(0)}, A^{(0)}, \gamma^{(0)})$, tolerance ϵ

Output: Estimated parameters $\boldsymbol{\nu} = (\pi, A, \gamma)$

- 1 **Initialize:** $m \leftarrow 0$
- 2 **repeat**
- 3 **E-step: Compute forward $\alpha_i(t)$ and backward $\beta_i(t)$:**
- 4 $\alpha_i(1) \leftarrow \pi_i^{(m)} \cdot \text{Poi}(J_1; \gamma_i^{(m)} I_1)$
- 5 **for** $t = 2, \dots, T$ **do**
- 6 $\alpha_i(t) \leftarrow \sum_j \alpha_j(t-1) A_{ji}^{(m)} \cdot \text{Poisson}(J_t; \gamma_i^{(m)} I_t)$
- 7 $\beta_i(T) \leftarrow \text{Poisson}(J_T; \gamma_i^{(m)} I_T)$
- 8 **for** $t = T-1, \dots, 1$ **do**
- 9 $\beta_i(t) \leftarrow \sum_j A_{ij}^{(m)} \cdot \text{Poisson}(J_{t+1}; \gamma_j^{(m)} I_{t+1}) \cdot \beta_j(t+1)$
- 10 $\mathbb{P}_{\boldsymbol{\nu}^{(m)}}(\theta_t = i \mid J_{1:T}) \leftarrow \frac{\alpha_i(t) \beta_i(t)}{\sum_k \alpha_k(t) \beta_k(t)}$
- 11 $\mathbb{P}_{\boldsymbol{\nu}^{(m)}}(\theta_t = i, \theta_{t+1} = j \mid J_{1:T}) \leftarrow \frac{\alpha_i(t) A_{ij}^{(m)} \text{Poisson}(J_{t+1}; \gamma_j^{(m)} I_{t+1}) \beta_j(t+1)}{\sum_{k, \ell} \alpha_k(t) A_{k\ell}^{(m)} \text{Poisson}(J_{t+1}; \gamma_\ell^{(m)} I_{t+1}) \beta_\ell(t+1)}$
- 12 **M-step: Update parameters using closed-form expressions:**
- 13 $\pi_j^{(m+1)} \leftarrow \mathbb{P}_{\boldsymbol{\nu}^{(m)}}(\theta_0 = j \mid J_{1:T})$
- 14 $A_{ij}^{(m+1)} \leftarrow \frac{\sum_{t=1}^{T-1} \mathbb{P}_{\boldsymbol{\nu}^{(m)}}(\theta_t = i, \theta_{t+1} = j \mid J_{1:T})}{\sum_{t=1}^{T-1} \mathbb{P}_{\boldsymbol{\nu}^{(m)}}(\theta_t = i \mid J_{1:T})}$
- 15 $\gamma_j^{(m+1)} \leftarrow \frac{\sum_{t=1}^T \mathbb{P}_{\boldsymbol{\nu}^{(m)}}(\theta_t = j \mid J_{1:T}) \cdot J_t}{\sum_{t=1}^T \mathbb{P}_{\boldsymbol{\nu}^{(m)}}(\theta_t = j \mid J_{1:T}) \cdot I_t}$
- 16 $m \leftarrow m + 1$
- 17 **until** $\|\boldsymbol{\nu}^{(m+1)} - \boldsymbol{\nu}^{(m)}\| < \epsilon$;

4.3. *Online Testing Procedure Controlling FDR.* We propose a modified version of Structure-Adaptive Sequential Testing (SAST; Gang, Sun and Wang, 2023), denoted as **SAST⁺**, tailored to temporally dependent and discrete data from hidden-state epidemic models. Unlike the original SAST, which assumes i.i.d. and continuous observations, **SAST⁺** incorporates parametric estimation and latent Markovian structure.

At each time T , we test the null hypothesis:

$$H_{0T} : \theta_T \in \{1(\text{decreasing}), 2(\text{stationary})\} \quad \text{vs.} \quad H_{1T} : \theta_T \in \{3(\text{increasing})\},$$

using the recent data window $J_{(T-h+1):T}$ of size h . We define the local null probability:

$$L_T(\boldsymbol{\nu}) = \mathbb{P}_{\boldsymbol{\nu}}(\theta_t \in \{1, 2\} \mid J_{(T-h+1):T}),$$

which quantifies the posterior probability that time t belongs to a non-increasing regime.

Since the parameter $\boldsymbol{\nu}$ is unknown, we estimate it using the EM algorithm (Algorithm 1) to obtain:

$$L_T(\hat{\boldsymbol{\nu}}_T) = \mathbb{P}_{\hat{\boldsymbol{\nu}}_T}(\theta_T \in \{1, 2\} \mid J_{(T-h+1):T}).$$

These values are computed for all $t \in \{T-h+1, \dots, T\}$, sorted in ascending order $L_{(1)} \leq \dots \leq L_{(h)}$, and used to define the adaptive threshold:

$$\hat{\lambda}_T = L_{(k)}, \quad \text{where } k = \max \left\{ t \leq h : \frac{1}{t} \sum_{i=1}^t L_{(i)} \leq \alpha \right\}.$$

We reject H_{0T} if:

1. $L_T(\hat{\nu}_T) \leq \hat{\lambda}_T$, and
2. The average of all rejected L_t 's including L_T does not exceed α :

$$\frac{1}{|\mathcal{R}_{T-1}| + 1} \left(\sum_{t \in \mathcal{R}_{T-1}} L_t(\hat{\nu}_t) + L_T(\hat{\nu}_T) \right) \leq \alpha.$$

This procedure avoids backward correction and uses only current estimates, ensuring real-time applicability. The full process is given in Algorithm 2.

Algorithm 2: SAST+

Input : Counts $J_{1:T}$, window size h , Significance level α

Output: Rejected set \mathcal{R}_T

- 1 **Initialization:**
 - 2 Estimate $\hat{\nu}_h$ using Algorithm 1 on $J_{1:h}$
 - 3 Compute $L_t(\hat{\nu}_h) = P_{\hat{\nu}_h}(\theta_t \in \{1, 2\} | J_{1:h})$ for $t = 1, \dots, h$
 - 4 Sort $\{L_t(\hat{\nu}_h)\}$ ascending: $L_{(1)}(\hat{\nu}_h) \leq \dots \leq L_{(h)}(\hat{\nu}_h)$
 - 5 Set $\hat{\lambda}_h \leftarrow \max \left\{ L_{(k)}(\hat{\nu}_h) : \frac{1}{k} \sum_{i=1}^k L_{(i)}(\hat{\nu}_h) \leq \alpha \right\}$
 - 6 Reject $H_{0(t)}$ if $L_t(\nu_T) \leq \hat{\lambda}_h$
 - 7 Set $\mathcal{R}_h = \{t \leq h : H_{0t} \text{ rejected}\}$
 - 8 **for** $T = h + 1, \dots, T$ **do**
 - 9 Estimate $\hat{\nu}_T$ from $J_{T-h+1:T}$ using Algorithm 1
 - 10 Compute $L_t(\hat{\nu}_T) = \mathbb{P}_{\hat{\nu}_T}(\theta_t \in \{1, 2\} | J_{T-h+1:T})$ for $t = T - h + 1, \dots, T$
 - 11 Sort $(L_t(\hat{\nu}_T))_{T-h+1 \leq t \leq T}$ ascending
 - 12 Set $\hat{\nu}_T \leftarrow \max \left\{ L_{(k)}(\hat{\nu}_T) : \frac{1}{k} \sum_{i=1}^k L_{(i)}(\hat{\nu}_T) \leq \alpha \right\}$
 - 13 **Reject** H_{0T} if both conditions hold:
 - 14 (C1) $L_T(\hat{\nu}_T) \leq \hat{\lambda}_T$,
 - 15 (C2) $\frac{1}{|\mathcal{R}_{T-1}| + 1} \left(\sum_{t \in \mathcal{R}_{T-1}} L_t(\hat{\nu}_t) + L_T(\hat{\nu}_T) \right) \leq \alpha$
 - 16 Update: $\mathcal{R}_T \leftarrow \mathcal{R}_{T-1} \cup \{T\}$ if rejected, else $\mathcal{R}_T \leftarrow \mathcal{R}_{T-1}$
-

4.4. *Theoretical Results.* We now present theoretical guarantees that support the use of this method under dependence. Under mild conditions, we show that the adaptive barrier $\hat{\lambda}_T$ is asymptotically the best gate-keeping threshold, and that SAST+ asymptotically controls FDR at the desired level.

To formalize this idea, we define the function $Q(\lambda)$, which quantifies the marginal false discovery proportion (FDP) when all hypotheses with LIS less than or equal to λ are rejected. Specifically,

$$Q(\lambda) = \frac{p_0 G_0(\lambda)}{G(\lambda)},$$

where

$$p_0 = \mathbb{P}(\theta_t \in \{1, 2\}), \quad G_0(\lambda) = \mathbb{P}(L_t(\nu) \leq \lambda | \theta_t \in \{1, 2\}), \quad G(\lambda) = \mathbb{P}(L_t(\nu) \leq \lambda).$$

Here, the numerator $p_0 G_0(\lambda)$ corresponds to the expected proportion of false discoveries (i.e., true nulls rejected) at threshold λ , and the denominator $G(\lambda)$ gives the overall rejection probability. Hence, $Q(\lambda)$ represents the expected FDP among all rejections made at that threshold.

The optimal barrier for FDR control is characterized by

$$\lambda^* = \sup \{ \lambda \in [0, 1] : Q(\lambda) \leq \alpha \}.$$

In offline settings—where all LIS values are known in advance—we can sort them and directly identify the largest rejection set that satisfies the FDR constraint. However, in online settings, only past LISs are observable at each step. This limited access leads to partial ordering and can cause inconsistencies: a hypothesis with a lower LIS may remain unrejected while one with a higher LIS is rejected.

To address this, SAST introduces a *barrier*—a gate-keeping threshold that restricts rejections to hypotheses with LIS values below a data-driven level (Gang, Sun and Wang, 2023). This threshold is updated adaptively based on observed LISs. Notably, the barrier itself does not need to exactly control the FDR. Instead, it is chosen to be slightly larger than the cutoff which controls FDR, providing higher power.

In the continuous setting—considered in Gang, Sun and Wang (2023)—the value λ^* corresponds to the largest threshold such that rejecting all hypotheses with $L_t(\boldsymbol{\nu}) \leq \lambda^*$ keeps the FDR within level α . We extend the role of barrier to the discrete setting, which commonly arises in practical applications. In such cases, λ^* may not exactly control FDR, and instead can be interpreted as the smallest one beyond which $Q(\lambda) > \alpha$.

THEOREM 4.1 (Adaptive Barrier). *Assuming the following assumptions hold:*

- A1** *The sequence of random variables θ_t forms a Markov chain that is irreducible, aperiodic, and stationary. This Markov chain is characterized by $\boldsymbol{\nu}_0$, which lies within the interior of the parameter space. Moreover, $\{J_t\}$ is also irreducible, aperiodic and stationary.*
- A2** *For any parameter set $\boldsymbol{\nu}$, let A represent the transition matrix and π denote the initial probability within set $\boldsymbol{\nu}$. Then, there exist $\delta > 0$ and $\epsilon > 0$ such that for all $\|\boldsymbol{\nu} - \boldsymbol{\nu}_0\| < \delta$ and $i, j = 1, 2, 3$, we have $A_{ij}, \pi_i > \epsilon$.*
- A3** *The maximum likelihood estimator $\hat{\boldsymbol{\nu}}$ is a consistent estimator of the true parameter set $\boldsymbol{\nu}_0$.*
- A4** *$Q(\lambda)$ is a decreasing function of λ .*

Applying Algorithm 2, the adaptive barrier obtained with significance level α satisfies at least one of the followings:

- *If $Q(\lambda^*) > \alpha$, then $\hat{\lambda}_T \xrightarrow{p} \lambda^*$ as $T \rightarrow \infty$ where \xrightarrow{p} represents the convergence in probability.*
- *If $Q(\lambda^*) = \alpha$, then for any $\epsilon > 0$, $\mathbb{P}(\hat{\lambda}_T \in [\underline{\lambda} - \epsilon, \lambda^* + \epsilon]) \rightarrow 1$ where $\underline{\lambda} = \inf\{\lambda : Q(\lambda) = \lim_{\epsilon \searrow 0} Q(\lambda^* - \epsilon)\}$.*

PROOF. The complete proof is presented in the supplementary material Section ?? □

THEOREM 4.2 (FDR control). *Assume that maximum likelihood estimator $\hat{\boldsymbol{\nu}}$ is a consistent estimate of true parameter set $\boldsymbol{\nu}_0$. Then Algorithm 2 allows for the control of the False Discovery Rate (FDR) of the entire sequence $(L_T(\hat{\boldsymbol{\nu}}_T))_{T=h+1, h+2, \dots}$ at a level of $\alpha + o(1)$.*

PROOF. The complete proof is provided in the supplementary material ?? □

5. Simulation Study. To evaluate our proposed method, simulations were performed under various setups. In addition, the effect of model misspecification was investigated to assess the robustness of our proposed models.

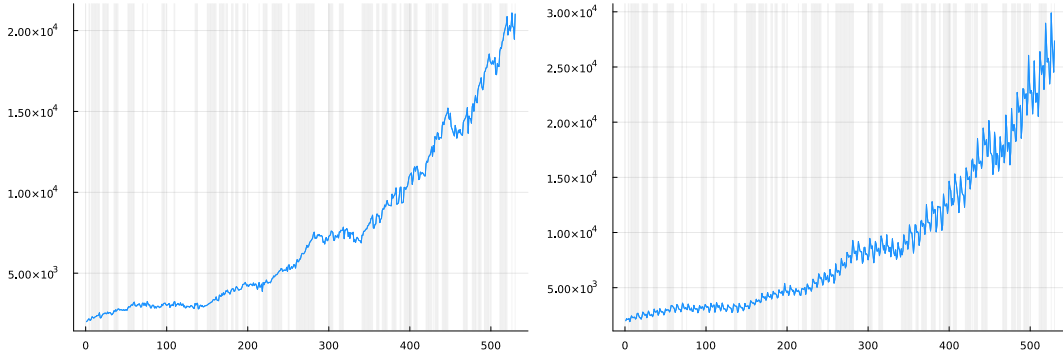


FIG 2. Generated data with a fixed seed ($seed = 1$) and parameter values $(\gamma_1, \gamma_2, \gamma_3) = (0.8, 1, 1.2)$. The left plot shows the trend without seasonal effects, while the right plot includes seasonal effects, highlighting periodic fluctuations. The shaded areas indicate periods of increasing values, representing days that should be rejected.

The infectious period, denoted as d , is established at 7 days. This value is typically well-established and disease-specific, so we assume that this period d is known. The transition matrix has been structured to favor its diagonal values as shown in (5.1). Unlike the infectious period d , we need to estimate the transition matrix denoted by \mathcal{A} which is set to be

$$(5.1) \quad \mathcal{A} = \begin{pmatrix} 0.60 & 0.30 & 0.10 \\ 0.05 & 0.80 & 0.15 \\ 0.05 & 0.15 & 0.80 \end{pmatrix}$$

to represent the slight increasing trend of J_t over time. Subsequently, we'll evaluate our proposed model with various configurations of γ_1 and γ_3 with $\gamma_2 = 1$ satisfying $\gamma_1 < 1 < \gamma_3$. Another consideration is to ensure the effective removal of any weekly cyclical patterns within our data. Although our approach presumes a successful adjustment of this periodicity, it's important to validate the effectiveness of such an adjustment. To denote the week periodicity, we referred to (4.1) which uses $\exp(S_t)$. Since we have $S_t = S_{t+d}$ for $d = 7$, we need only (S_1, S_2, \dots, S_7) which are corresponding to (Mon, Tues, ..., Sun). We use

$$(5.2) \quad (S_1, S_2, \dots, S_7) = \left(\frac{1}{10}, \frac{1}{20}, 0, 0, 0, -\frac{1}{10}, -\frac{1}{20} \right)$$

for modeling the weekly effect. The reason for providing these values is that the number of tests is lowest on weekends, resulting in the lowest reported number of disease cases. On the other hand, there is often a rebound in reported cases over the next two days (Monday and Tuesday). From Wednesday to Friday, the number of cases tends to remain relatively stable. These fluctuations are assumed to be unknown and their effects are removed after estimation.

The Figure 2 illustrates the generated data with a fixed random seed ($seed = 1$) and parameter values $(\gamma_1, \gamma_2, \gamma_3) = (0.8, 1, 1.2)$. The plot on the left shows the trend of the data without seasonal effects, providing a clear baseline representation of the underlying trend. In contrast, the plot on the right incorporates seasonal effects, highlighting periodic fluctuations superimposed on the trend. Additionally, the shaded areas in both plots indicate periods of increasing that should be rejected. This side-by-side comparison emphasizes the impact of seasonal components on the data and how they interact with the overall trend. We consider the situation that data come in online over a period of 530 days, and the simulation will be repeated 500 times to compare the FDR and the statistical power of tests such as TPR(True Positive Rate) which is defined in the following section. Our proposed methods are applied with the same window size $h = 30$.

We test the hypotheses H_{0T} for $31 \leq T \leq 530$ where each hypothesis H_{0T} is tested based on the data observed $J_{1:T} = \{J_1, \dots, J_T\}$.

5.1. *Simulation Results of Online Testing* . Without seasonal effect, different parameter set-ups are considered: $(\gamma_1, \gamma_2, \gamma_3) = (0.8, 1, 1.2), (0.85, 1, 1.15), (0.9, 1, 1.1)$ and $(0.95, 1, 1.05)$. As the difference $\gamma_3 - \gamma_1$ is smaller, it is more difficult to distinguish the null and alternative hypotheses. Table 1-2 shows the estimated FDR and power, the True Positive Rate (TPR) which has the following definition :

$$(5.3) \quad TPR = E \left(\frac{\sum_{t \in \mathcal{R}_T \cap \{31, 32, \dots, 530\}} I(\theta_t = 3)}{(\sum_{t=31}^{530} I(\theta_t = 3)) \vee 1} \right)$$

and an estimator of TPR denoted by \widehat{TPR} is obtained from Monte Carlo simulation.

These results have been compared with

- an ‘oracle’ setting where all parameters in ν defined in (4.1) are known and tested in offline setting with all 530 data is observed at once,
- Existing online FDR-controlling procedures, including LORD++ (Ramdas et al., 2017a), SAFFRON (Ramdas et al., 2018), and ADDIS (Tian and Ramdas, 2019), which operate on p -values. For these methods, we compute the p -value at each time t as

$$p_t = 1 - F_{I_t}(J_t),$$

where F_{I_t} denotes the cumulative distribution function (CDF) of the Poisson distribution with mean I_t . Note that these p -value-based methods do not guarantee FDR control at level α in the presence of temporal dependence, which is inherent in our application setting.

Combining with the proposed online procedures, SAST+, the FDR is generally well controlled for most parameter settings in Table 1, and the estimated powers (\widehat{TPR}) are slightly lower than those of the oracle procedure. Online testing methods based on p -values show comparable power with SAST+ in most cases except the case when $(\gamma_1, \gamma_2, \gamma_3) = (0.95, 1, 1.05)$.

Due to the presence of seasonal effects, decision-making becomes more challenging, as demonstrated by the oracle procedures in Table 2. Consequently, the FDR increases across all methods. Among these, LORD++, SAFFRON, and ADDIS fail to control the FDR, while SAST+ successfully controls the FDR at the target level of $\alpha = 0.05$, except in cases where the true γ_i values are closely aligned. This suggests that the STL decomposition may contribute to increased noise.

TABLE 1
Simulation results without seasonal effects.

$(\gamma_1, \gamma_2, \gamma_3)$	Oracle		SAST+		LORD		SAFFRON		ADDIS	
	\widehat{FDR}	\widehat{TPR}								
(0.8, 1, 1.2)	0.000	1.000	0.000	1.000	0.004	1.000	0.031	1.000	0.042	1.000
(0.85, 1, 1.15)	0.001	1.000	0.000	1.000	0.004	1.000	0.032	1.000	0.042	1.000
(0.9, 1, 1.1)	0.015	1.000	0.001	0.998	0.004	0.993	0.032	0.998	0.042	0.998
(0.95, 1, 1.05)	0.058	0.978	0.045	0.931	0.004	0.650	0.031	0.837	0.041	0.839

TABLE 2
Simulation results with seasonal effects

$(\gamma_1, \gamma_2, \gamma_3)$	Oracle		SAST+		LORD		SAFFRON		ADDIS	
	\widehat{FDR}	\widehat{TPR}								
(0.8, 1, 1.2)	0.024	0.979	0.038	0.985	0.296	0.999	0.316	0.999	0.333	1.000
(0.85, 1, 1.15)	0.028	0.982	0.036	0.985	0.255	0.997	0.285	0.998	0.309	0.999
(0.9, 1, 1.1)	0.050	0.983	0.042	0.977	0.169	0.977	0.218	0.989	0.251	0.992
(0.95, 1, 1.05)	0.082	0.936	0.090	0.897	0.034	0.640	0.091	0.806	0.109	0.824

5.2. *Simulation Results of Seasonal Effect Adjustment.* Although seasonal adjustment is not our primary concern, it can still influence our decisions. To evaluate the impact of seasonal adjustment, we ran an additional simulations under misspecified seasonal effect: We tested the FDR and TPR under misspecified seasonal effects. This involved generating J_t with seasonal effects but not adjusting for them prior to estimation, and vice versa.

TABLE 3

Simulation results with mismatch in the presence of seasonal effect (S/E). (+) indicates the presence of S/E and (-) indicates no S/E. Results with correctly specified S/E are shown in bold.

True S/E	Specified S/E	Oracle		SAST+		LORD		SAFFRON		ADDIS	
		\overline{FDR}	\overline{TPR}								
-	-	0.000	1.000	0.000	1.000	0.090	1.000	0.113	1.000	0.172	1.000
	+	0.022	0.995	0.022	0.976	0.026	0.874	0.054	0.917	0.076	0.934
+	-	0.209	0.797	0.197	0.724	0.193	0.761	0.201	0.810	0.219	0.814
	+	0.019	0.947	0.042	0.974	0.219	0.999	0.246	0.999	0.287	1.000

Table 3 shows the results of the model analysis in scenarios where seasonal effects are either (i) present and unadjusted, or (ii) absent but adjusted. The results show that accounting for seasonal effects in the absence of actual seasonal effects increase the FDR and decrease TPR slightly. Conversely, omitting seasonal adjustment can significantly inflate the FDR while reducing the TPR. These results highlight the importance of appropriately adjusting for seasonal effects in the model, and demonstrate that our adjustment of seasonal effect produces robust results even in the absence of seasonal effects.

6. Real Data Analysis. To evaluate the empirical performance and operational boundaries of our proposed method (SAST+), we apply it to a diverse set of real-world infectious disease surveillance datasets. These datasets were chosen to represent a range of transmission dynamics and data granularities. We first validate the method’s effectiveness on high-resolution daily COVID-19 data, which closely aligns with our model’s assumptions. We then critically examine its robustness and limitations for diseases with different epidemiological characteristics. The performance of SAST+ is benchmarked against three established online FDR-controlling procedures: LORD++, SAFFRON, and ADDIS.

6.1. *Performance Validation on High-Resolution Data: The Case of COVID-19.* Our primary validation is conducted using daily COVID-19 incidence data, which offers the highest temporal resolution and aligns well with our model’s assumptions of a human-to-human transmitted pathogen. We analyze daily data from Australia and South Korea, obtained from the Our World in Data (OWID) repository (Mathieu et al., 2020). Daily data often exhibits strong periodic effects, such as reduced reporting over weekends. To address this, we apply an online STL decomposition as described in Section 4.1, using a 30-day window at each time point to remove the weekday reporting bias before analysis. We set the infectious period to $d = 7$ days and the smoothing window size to $h = 30$ days.

Figures 3 and 4 show the daily number of infectious individuals for Australia and South Korea, respectively, alongside the rejection times identified by four online FDR-controlling procedures. The top panel displays the raw data, while the second panel shows the same data on a **log scale**, smoothed with a 7-day moving average.

In Australia (Figure 3), two major epidemic waves are observed: one from May to October 2020 and another from June to October 2021. The first wave, from May to October 2020, centered in Victoria, resulted from breaches in hotel quarantine protocols, peaking in early August. During this period, SAST+ generated early and sustained rejections, effectively capturing the outbreak onset ahead of other methods. A second major wave, from June

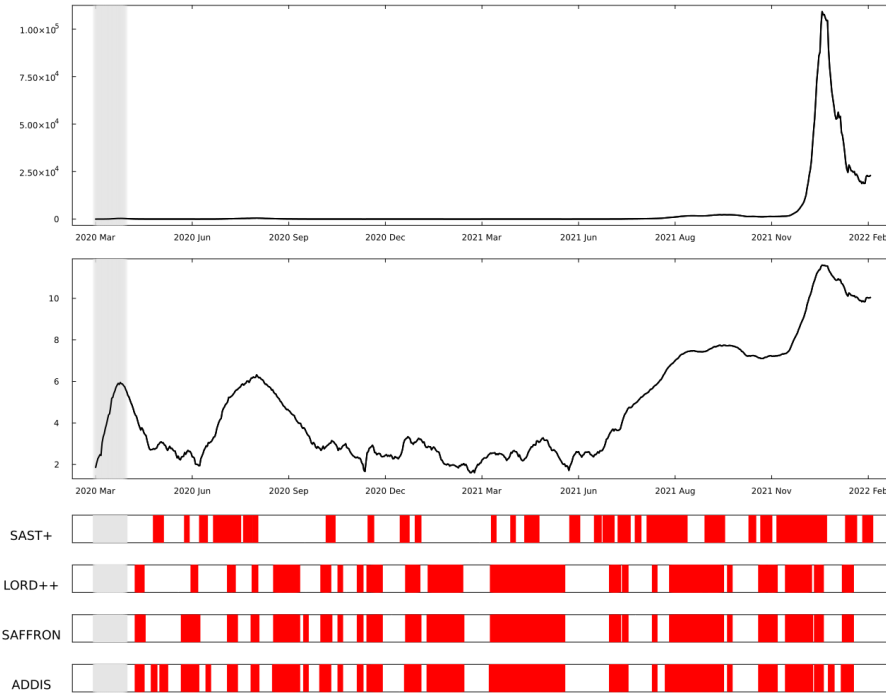


FIG 3. Online FDR analysis of daily infectious counts (J_t) in Australia. The top two panels show the raw and the log-scaled/smoothed data, respectively. Grey areas mark training periods. The lower four panels show the results for four different online FDR procedures, with red markers indicating rejection times.

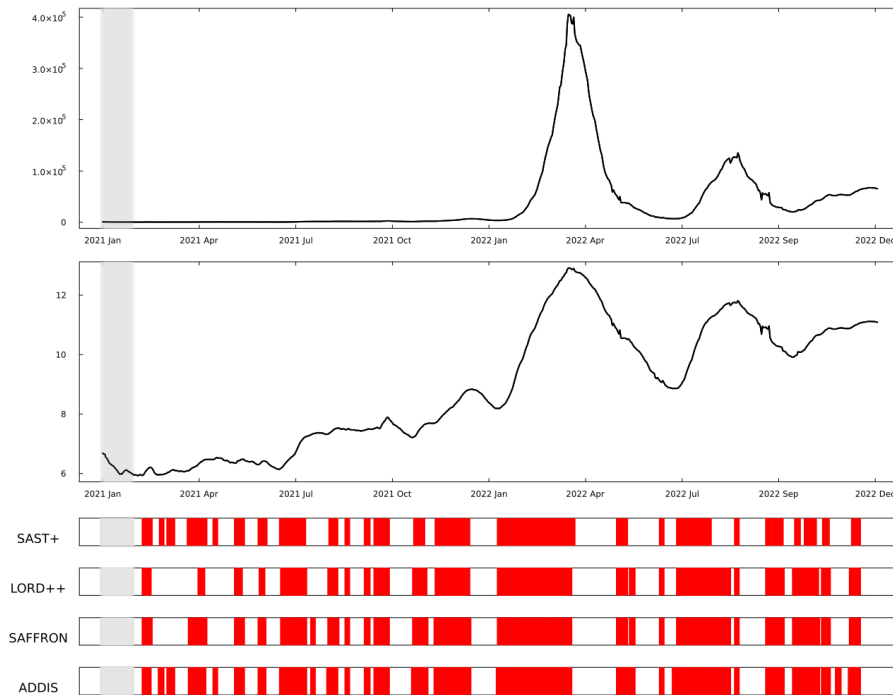


FIG 4. Online FDR analysis of daily infectious counts (J_t) in South Korea. The top two panels show the raw and the log-scaled/smoothed data, respectively. Grey areas mark training periods. The lower four panels show the results for four different online FDR procedures, with red markers indicating rejection times.

to October 2021, triggered by the Delta variant, was also promptly identified by SAST+, with rejections aligned with the early growth of the outbreak.

Interestingly, between these waves, SAST+ made additional rejections in response to fluctuations in imported case risk (e.g., from India in April 2021), where other methods remained inactive. This highlights SAST+'s sensitivity to subtle but epidemiologically meaningful trends.

In South Korea (Figure 4), the first major outbreak occurred in August 2020 due to church clusters and mass gatherings. This was followed by a large Alpha-variant-driven wave in December 2020 and a Delta-driven surge in mid-2021. In all three episodes, SAST+ detected early and temporally coherent blocks of rejections. Notably, the method adapted its rejection pattern in response to intensified public health interventions such as distancing mandates, with rejection rates declining as case counts stabilized.

Overall, these results highlight the adaptive effectiveness of SAST+. While SAST+ clearly outperformed competing methods in coherence and sensitivity during Australia's shifting epidemic, its distinct advantage was less pronounced in South Korea, where all methods yielded satisfactory and comparable results in identifying outbreak phases.

6.2. Robustness to Reporting Mechanism. We analyze two diseases that have different reporting requirements to that of COVID-19: *Mycoplasma pneumoniae* and influenza.

Mycoplasma Pneumoniae and *Influenza* in Korea are designated as Class 4 infectious diseases, requiring reporting within one week. This introduces potential delays and lower data precision compared to the daily COVID-19 dataset. For *Mycoplasma Pneumoniae*, with an infectious period of 2-4 weeks ([New York State Department of Health](#)), we set $d = 3$ and $h = 15$ weeks. For *Influenza*, with a typical 7-day infectious period ([Centers for Disease Control and Prevention, 2023](#)), we conservatively set $d = 2$ and $h = 8$ weeks. As shown in Figures 5 and 6, SAST+ effectively identifies key outbreak periods. For *Mycoplasma*, it makes the most rejections (51) and best captures prolonged increasing trends. For *Influenza*, its detections (34) form more connected blocks during surges than the more fragmented discoveries of other methods. This affirms the method's utility for standard public health surveillance systems that rely on weekly reporting.

Robustness to Model Misspecification: Application to an SIR-Type Disease

To challenge the foundational assumptions of our proposed method, we test its performance on data for Chickenpox, a disease whose transmission dynamics represent a technical violation of our model's framework. Our method is designed based on the Susceptible-Infectious-Susceptible (SIS) model, which assumes that individuals return to the susceptible state after recovering from an infection. This framework is well-suited for diseases that do not confer long-term immunity.

In contrast, Chickenpox confers lifelong immunity upon recovery, making it a classic example of a disease best described by the Susceptible-Infectious-Recovered (SIR) model [Kermack and McKendrick \(1927b\)](#). The SIR model, originally developed by Kermack and McKendrick, compartmentalizes a population into three distinct groups: Susceptible (S), individuals who can contract the disease; Infectious (I), those who currently have the disease and can transmit it; and Recovered (R), individuals who have recovered and are now permanently immune. The key distinction from the SIS model is the transition from the Infectious to the Recovered compartment, which removes individuals from the pool of potential future infections.

Despite this model mismatch, we posit that an SIS framework can serve as a robust approximation for an SIR-type disease under common real-world conditions. The force of infection in our model is approximated by the term $(S_t/N)\gamma_t I_t$. In a large population (N) where the number of active cases (I_t) is relatively small, the susceptible pool (S_t) depletes very slowly.

Consequently, the ratio S_t/N remains approximately equal to 1 for extended periods, making the simplification acceptable.

Furthermore, demographic changes such as births and deaths introduce a natural flux to the population. In many scenarios, the introduction of new susceptible individuals into the population via births can have a more significant impact on the susceptible pool than its depletion due to infections alone. This demographic turnover partially mimics the feedback loop of an SIS model by replenishing the susceptible class, thereby mitigating the conceptual violation of the model’s assumptions.

For our analysis of Chickenpox, a Class 2 notifiable disease in Korea with a typical infectious period of 5–7 days ([Centers for Disease Control and Prevention](#)), we set our model parameters to a 1-week infectious period ($d = 1$) and a 4-week seasonality horizon ($h = 4$). The results, illustrated in Figure 7, show that our SAST+ method successfully captures the recurrent surges in cases with connected blocks of rejections (64). This outcome demonstrates the method’s robustness and practical utility even when the underlying disease dynamics do not perfectly align with the theoretical SIS framework.

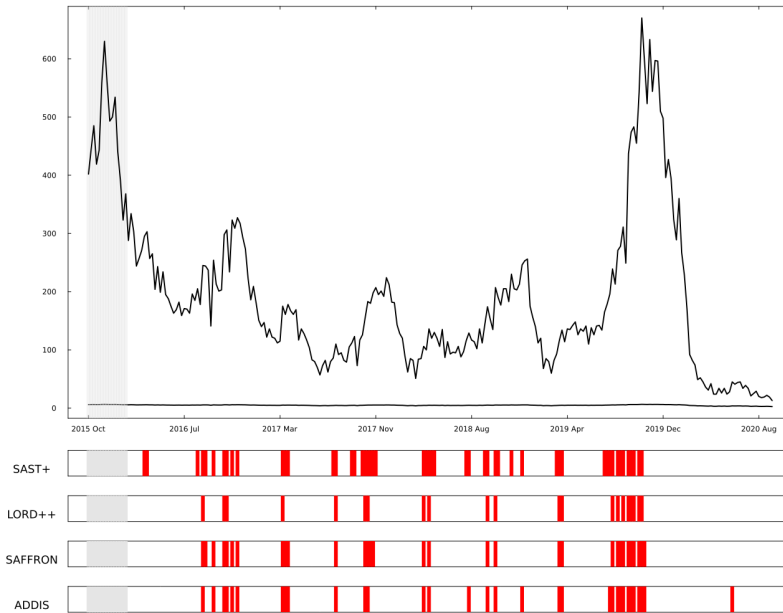


FIG 5. J_t of *Mycoplasma Pneumoniae* in South Korea with 15 weeks of training periods (grey), and rejections by online FDR controlling procedures (red).

Robustness to a Vector-borne Disease

We investigate a boundary condition where the core assumption of human-to-human transmission is violated. We analyze weekly Dengue Fever data from Singapore ([Ministry of Health, Singapore, 2024](#)), a vector-borne disease transmitted by mosquitoes. In this case, the SIS model is ill-suited because the force of infection is not primarily driven by the number of infectious humans (I_t) but by external factors like the vector population density, climate, and biting rates, which our model does not include. We set $d = 2$ and $h = 8$ weeks to account for the viremic period ([World Health Organization, 2024](#)) and reporting lags. While SAST+ identifies the most potential signals (71) in Figure 8, their alignment with outbreak surges is less consistent than for the directly transmitted diseases.

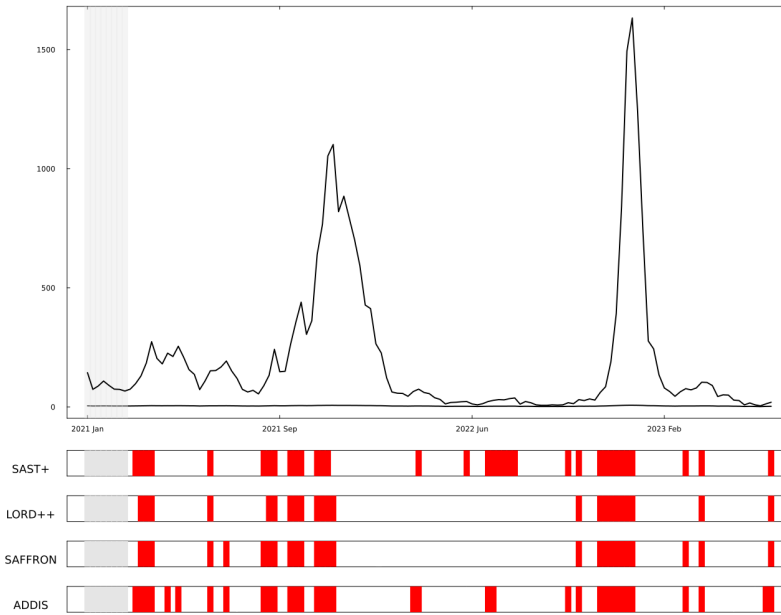


FIG 6. J_t of Influenza in South Korea with 8 weeks of training periods (grey), and rejections by online FDR controlling procedures (red).

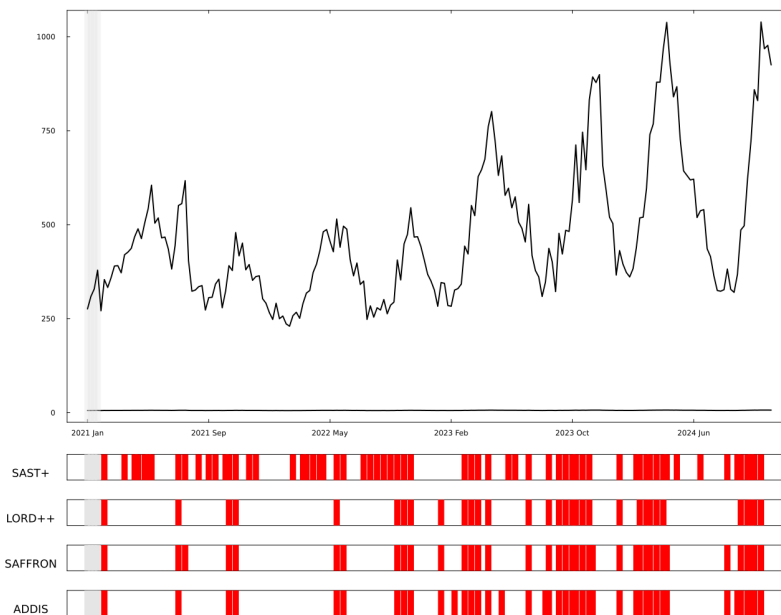


FIG 7. J_t of Chickenpox in South Korea with 4 weeks of training periods (grey), and rejections by online FDR controlling procedures (red).

This observation highlights a key limitation of applying an SIS-based framework to this class of infections. The epidemiology of vector-borne diseases is defined by an indirect transmission cycle that requires modeling the vector population itself (Ross, 1911). State-of-the-art models are therefore complex, often incorporating detailed data on vector ecology and environmental conditions (Focks et al., 1995; Andraud et al., 2012). Our method, based on

a direct-transmission model, cannot account for these external factors, which weakens its ability to detect surges driven by vector dynamics.

This finding helps define the scope of our method. It covers many settings even the infectious diseases with lifelong immunity, but may have limited applicability for some vector-borne diseases, where more specialized models are needed for optimal performance.

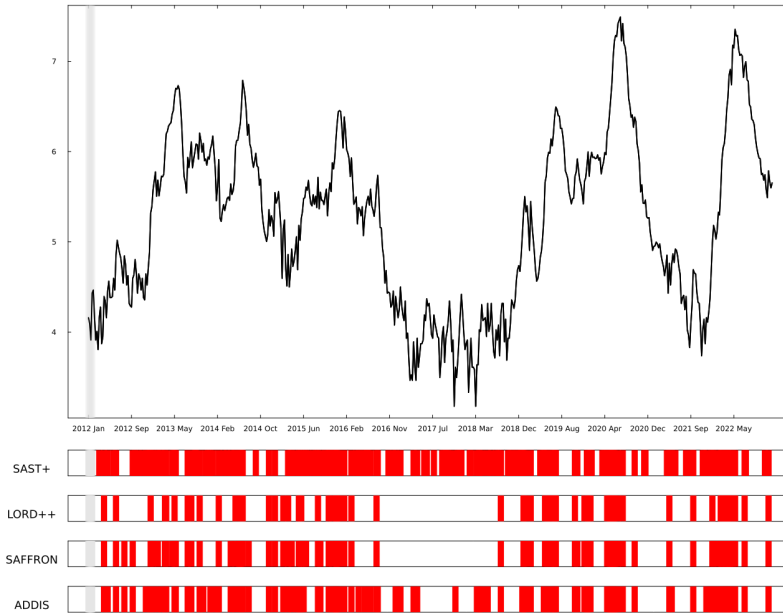


FIG 8. J_t of Dengue in Singapore with 8 weeks of training periods (grey), and rejections by online FDR controlling procedures (red).

7. Concluding Remarks. Compared to the traditional SIS method, our approach adopts a probabilistic perspective on epidemiological events rather than the standard deterministic approach. By transforming an SIS model into a Poisson (or binomial) distribution, we can improve the interpretability between consecutive numbers of infectious people. In addition to the statistical SIS model, we suggest online FDR control method, SAST+, which test whether the number of infected individuals tends to increase or not and showed that this procedure can control FDR in online environment.

This procedure is compared with some existing methods which handle online data designed for controlling any given FDR. The numerical studies show that only SAST+ controls FDR and shows comparable power with oracle procedure if the model is true.

Our empirical evaluation on real-world data demonstrated the practical utility and operational scope of SAST+. On high-resolution COVID-19 data, our method showed a distinct advantage over traditional change-point detection methods by effectively identifying sustained transmission trends over long periods, a known limitation of methods designed to find only a single change point. Furthermore, our analyses extended beyond this ideal scenario. SAST+ demonstrated strong robustness, performing effectively on standard weekly surveillance data for Influenza and Mycoplasma pneumoniae, and even when applied to Chickenpox, a disease better described by an SIR model. Crucially, the study also defined the method's boundaries. The analysis of Dengue Fever, a vector-borne disease, highlighted the limitations of the SIS-based framework for indirect transmission routes, where performance was attenuated.

Taken together, these real-world applications not only validate the effectiveness of SAST+ for monitoring human-to-human infectious diseases but also transparently establish its scope of application. These innovations make our methods not only accurate and reliable for analyzing trends in diseases like COVID-19 but also highly adaptable for wider applications in public health surveillance.

As future work, we assumed stationary processes which may be somewhat strong condition, so it is of interest to extend the methods to non-stationary processes.

Supplementary materials. Supplementary materials include the detailed explanation of EM algorithm and the proofs of all Theorems and Lemmas.

Funding. This work was supported by the National Research Foundation of Korea (NRF) grant funded by the Korea government (MSIT) (RS-2025-00556575).

Conflict of Interest. The authors have declared no conflict of interest.

8. Data and Code Availability. The COVID-19 dataset(OWID) and source code of this paper can be found at the following GitHub repository: https://github.com/IAMSHHWANG/statistical_SIS.

REFERENCES

- ANDRAUD, M., HENS, N., MARA, V. K. and BEUTELS, P. (2012). Dynamic models of dengue transmission: a systematic review of the literature. *PLoS neglected tropical diseases* **6** e1859.
- CLEVELAND, R. B., CLEVELAND, W. S., MCRAE, J. E., TERPENNING, I. et al. (1990). STL: A seasonal-trend decomposition. *J. Off. Stat* **6** 3–73.
- EFRON, B. (2005). Local false discovery rates.
- FOCKS, D. A., DANIELS, E., HAILE, D. G. and KEESLING, J. E. (1995). A dynamic life table model for *Aedes aegypti* (Diptera: Culicidae): simulation results and validation. *Journal of medical entomology* **32** 293–302.
- CENTERS FOR DISEASE CONTROL AND PREVENTION Chickenpox (Varicella) – Transmission. Accessed: 2025-07-20.
- CENTERS FOR DISEASE CONTROL AND PREVENTION (2023). How Flu Spreads. Accessed: 2025-07-20.
- FOSTER, D. P. and STINE, R. A. (2008). α -investing: a procedure for sequential control of expected false discoveries. *Journal of the Royal Statistical Society Series B: Statistical Methodology* **70** 429–444.
- GANG, B., SUN, W. and WANG, W. (2023). Structure-adaptive sequential testing for online false discovery rate control. *Journal of the American Statistical Association* **118** 732–745.
- KERMACK, W. O. and MCKENDRICK, A. G. (1927a). A contribution to the mathematical theory of epidemics. *Proceedings of the Royal Society of London. Series A, Containing Papers of a Mathematical and Physical Character* **115** 700–721.
- KERMACK, W. O. and MCKENDRICK, A. G. (1927b). A Contribution to the Mathematical Theory of Epidemics. *Proceedings of the Royal Society of London. Series A, Containing Papers of a Mathematical and Physical Character* **115** 700–721. <https://doi.org/10.1098/rspa.1927.0118>
- KOLLER, D. and FRIEDMAN, N. (2009). *Probabilistic graphical models: principles and techniques*. MIT press.
- MATHIEU, E., RITCHIE, H., RODÉS-GUIRAO, L., APPEL, C., GIATTINO, C., HASELL, J., MACDONALD, B., DATTANI, S., BELTEKIAN, D., ORTIZ-OSPINA, E. and ROSER, M. (2020). Coronavirus Pandemic (COVID-19). <https://ourworldindata.org/coronavirus>. Accessed: 2022-12-12.
- MINISTRY OF HEALTH, SINGAPORE (2024). Weekly Infectious Disease Bulletin Cases. Government of Singapore. Retrieved August 6, 2025, from <https://data.gov.sg/dataset/weekly-infectious-disease-bulletin-cases>.
- MURPHY, K. P. (2002). *Dynamic bayesian networks: representation, inference and learning*. University of California, Berkeley.
- NEW YORK STATE DEPARTMENT OF HEALTH Mycoplasma Infection (walking pneumonia, atypical pneumonia) Fact Sheet. Website. Accessed: 2025-07-28. Page last reviewed: November 2023.
- WORLD HEALTH ORGANIZATION (2024). Dengue and severe dengue. Fact sheet. Retrieved August 6, 2025, from <https://www.who.int/news-room/fact-sheets/detail/dengue-and-severe-dengue>.
- RAMDAS, A., YANG, F., WAINWRIGHT, M. J. and JORDAN, M. I. (2017a). Online control of the false discovery rate with decaying memory. *Advances in neural information processing systems* **30**.

- RAMDAS, A., YANG, F., WAINWRIGHT, M. J. and JORDAN, M. I. (2017b). Online control of the false discovery rate with decaying memory. *Advances in neural information processing systems* **30**.
- RAMDAS, A., ZRNIC, T., WAINWRIGHT, M. and JORDAN, M. (2018). SAFFRON: an adaptive algorithm for online control of the false discovery rate. In *International conference on machine learning* 4286–4294. PMLR.
- ROSS, R. (1911). The prevention of malaria. *Nature* **88** 51–52.
- SUN, W. and CAI, T. T. (2007). Oracle and adaptive compound decision rules for false discovery rate control. *Journal of the American Statistical Association* **102** 901–912.
- TIAN, J. and RAMDAS, A. (2019). ADDIS: an adaptive discarding algorithm for online FDR control with conservative nulls. *Advances in neural information processing systems* **32**.